

# Analysis of $K_L \rightarrow \gamma\nu\bar{\nu}$

S. Richardson and C. Picciotto

*Department of Physics and Astronomy, University of Victoria, Victoria, British Columbia,  
Canada V8W 3P6*

(August 30, 2018)

## Abstract

The decay  $K_L \rightarrow \gamma\nu\bar{\nu}$  is analyzed within the standard model. Short-distance contributions are found to dominate, yielding a branching ratio of  $\sim 0.7 \times 10^{-11}$ . We examine the possibility that non-standard model effects might be observed at higher rates. As an example, we calculate the branching ratio for the process mediated by neutral horizontal gauge bosons. Notwithstanding some model uncertainties, experimental limits for lepton number violation constrains these contributions to  $\lesssim 2 \times 10^{-11}$ .

(Accepted for publication in Physical Review D)

arXiv:hep-ph/9509372v1 22 Sep 1995

Typeset using REVTeX

## I. INTRODUCTION

Rare kaon decays continue to be an area of active research [1]. Within the standard model, rare decays are governed by loop level processes and thus directly probe the quantum structure of the theory. Experimental searches serve several complementary purposes. Improved limits help to constrain standard-model parameters, while discovery of clear discrepancies with standard-model predictions would signal new physics. Proposed extensions to the standard model are similarly constrained.

Of particular interest are rare decays which are dominated by short-distance contributions and hence are free of theoretical uncertainties from long-distance effects. A well-known example is  $K^+ \rightarrow \pi^+ \nu \bar{\nu}$  [2–4]. This decay is expected to give a clean determination of the Kobayashi-Maskawa matrix element  $V_{td}$ , provided the top quark mass is well-known. Another example is  $K_L \rightarrow \pi^0 \nu \bar{\nu}$  [2,5], which is of special interest because its dominant contribution is expected to arise from direct  $CP$  violation.

A rare kaon decay which has not been well-studied is  $K_L \rightarrow \gamma \nu \bar{\nu}$ . Although the reasons for its study are perhaps not as compelling as those for the previous two processes, it is just as important to test this decay for consistency with standard-model predictions; as noted above, rare processes with very low rates are fertile ground in which to look for non-standard effects. Furthermore, information about this process will be useful in background analysis of other rare-decay experiments. An early calculation by Ma and Okada [6] predicted a negligible branching ratio of  $\sim 10^{-18}$ . Their calculation, however, predates the confirmation of the 3rd quark family and clearly needs to be updated. In Sec. II we examine some long-distance processes and find contributions up to  $0.7 \times 10^{-12}$ . Short-distance effects are considered in Sec. III, and we find a branching ratio of  $0.7 \times 10^{-11}$ . Thus within the standard model  $K_L \rightarrow \gamma \nu \bar{\nu}$  also appears to be short-distance dominated.

One of the defining characteristics of the standard model is the absence of tree-level flavor-changing neutral currents (FCNC). However, many proposed extensions (technicolor theories for example) predict such currents. Rare neutral current kaon decays provide an ideal window to look for such effects. In Sec. IV we consider possible FCNC contributions that could arise from neutral generation-changing gauge bosons. Our concluding remarks appear in Sec. V.

## II. LONG-DISTANCE

The two long-distance contributions we consider are shown in Fig. 1. Momentum and polarization assignments are indicated on the graphs. Each contribution is treated separately below. Note that within the standard model the form of the  $K_L \rightarrow \gamma \nu \bar{\nu}$  decay amplitude is tightly constrained by Lorentz and electromagnetic gauge invariance. Assuming  $CP$  conservation, the only allowed form is

$$\varepsilon^{\mu\nu\rho\sigma} (\bar{u} \gamma_\mu P_L v) k_\nu \epsilon_\rho p_\sigma, \quad (1)$$

where  $\bar{u}$  and  $v$  are neutrino spinors, and  $P_L = (1 - \gamma^5)/2$ .

### A. $K_L \rightarrow P \rightarrow \gamma\nu\bar{\nu}$

We first consider the long-distance diagrams shown in Fig. (1)(a). They involve a weak transition of the kaon to a virtual pseudoscalar meson  $P = \pi^0, \eta, \eta'$ . The corresponding amplitude  $A$  can be written in the form

$$A = \frac{\sqrt{2}\langle\gamma\nu\bar{\nu}|\mathcal{H}|\pi^0\rangle\langle\pi^0|\mathcal{H}|K^0\rangle}{m_K^2 - m_{\pi^0}^2}(1 + A_\eta + A_{\eta'}), \quad (2)$$

assuming  $\langle P|\mathcal{H}|K^0\rangle = \langle P|\mathcal{H}|\bar{K}^0\rangle$ . The quantities  $A_\eta$  and  $A_{\eta'}$  represent the contributions of the  $\eta$  and  $\eta'$  diagrams relative to the pion graph amplitude. Their kaon transition elements, for example  $\langle\eta|\mathcal{H}|K^0\rangle$ , can be related to the corresponding  $\pi^0$  transition element using SU(3) flavor symmetry. To account for interference effects, we carefully treat symmetry breaking [7]. We use the mixing convention

$$|\eta\rangle = \cos\theta|\eta_8\rangle - \sin\theta|\eta_0\rangle, \quad (3a)$$

$$|\eta'\rangle = \sin\theta|\eta_8\rangle + \cos\theta|\eta_0\rangle, \quad (3b)$$

where  $\eta_8$  and  $\eta_0$  denote the usual SU(3) octet and singlet states. The kaon transitions then satisfy,

$$\frac{\langle\eta_8|\mathcal{H}|K^0\rangle}{\langle\pi^0|\mathcal{H}|K^0\rangle} = \frac{1}{\sqrt{3}}(1 + \zeta), \quad (4a)$$

$$\frac{\langle\eta_0|\mathcal{H}|K^0\rangle}{\langle\pi^0|\mathcal{H}|K^0\rangle} = -\sqrt{\frac{8}{3}}\rho, \quad (4b)$$

where  $\zeta$  and  $\rho$  parameterize SU(3) breaking. Current algebra gives  $\langle\pi^0|\mathcal{H}|K^0\rangle \simeq 1 \times 10^{-7} m_K^2$  [7]. Chiral perturbation theory to one loop predicts  $\zeta \simeq 0.17$  [7]. The singlet parameter  $\rho$  and mixing angle  $\theta$  are fit to experiment. We will take  $\rho = 0.83$  and  $\theta = -20.6^\circ$  [8].

The pseudoscalar transitions  $\langle\gamma\nu\bar{\nu}|\mathcal{H}|P\rangle$  can be described by constituent quark triangle diagrams [9], shown in Fig. 2. The calculation mimics the well-known triangle graph approach to  $\pi^0 \rightarrow \gamma\gamma$  [10]. We obtain

$$\langle\gamma\nu\bar{\nu}|\mathcal{H}|P\rangle = \frac{eG_F}{\sqrt{2}\pi^2} I_P \varepsilon^{\mu\nu\rho\sigma} (\bar{u}\gamma_\mu P_L v) k_\nu \epsilon_\rho p_\sigma, \quad (5)$$

where the pseudoscalar and quark loop dependencies have been collected into the coefficients  $I_P$ . It is convenient to express  $I_P$  in terms of the mass ratios  $\xi_q \equiv p^2/m_q^2$  for constituent quark flavor  $q$ . Then

$$I_P = 2N_c \sum_q Q_q \frac{g_{Pq\bar{q}}}{m_q} \frac{c_{Vq}}{\xi_q} \left( \arcsin \sqrt{\xi_q/4} \right)^2, \quad (6)$$

provided  $0 \leq \xi_q \leq 4$ . Here  $N_c = 3$  is the number of colors,  $Q_q$  are the quark charges in units of  $e$ , and  $c_{Vq}$  are the standard-model weak vector coupling coefficients. The effective meson-quark couplings  $g_{Pq\bar{q}}$  are shown in Table I. The parameters  $f_8 = 1.25f_\pi$  and  $f_0 = 1.04f_\pi$ , where  $f_\pi = 132$  MeV, account for SU(3) breaking in the  $\eta_8$  and  $\eta_0$  amplitudes [11]. For the

constituent quark masses, we choose the representative values  $m_u = m_d = 0.31$  GeV and  $m_s = 0.46$  GeV. The resulting coefficient values are  $I_{\pi^0} = 0.25$ ,  $I_{\eta_8} = 0.51$ , and  $I_{\eta_0} = 5.7$  GeV<sup>-1</sup>.

In terms of Eqs. (3), (4) and (6), the quantities  $A_\eta$  and  $A_{\eta'}$  are

$$A_\eta = \frac{m_K^2 - m_{\pi^0}^2}{m_K^2 - m_\eta^2} \left( \frac{I_{\eta_8}}{I_{\pi^0}} \cos \theta - \frac{I_{\eta_0}}{I_{\pi^0}} \sin \theta \right) \times \left( \frac{1 + \zeta}{\sqrt{3}} \cos \theta + \sqrt{\frac{8}{3}} \rho \sin \theta \right), \quad (7a)$$

$$A_{\eta'} = \frac{m_K^2 - m_{\pi^0}^2}{m_K^2 - m_{\eta'}^2} \left( \frac{I_{\eta_8}}{I_{\pi^0}} \sin \theta + \frac{I_{\eta_0}}{I_{\pi^0}} \cos \theta \right) \times \left( \frac{1 + \zeta}{\sqrt{3}} \sin \theta - \sqrt{\frac{8}{3}} \rho \sin \theta \right). \quad (7b)$$

Inserting the numerical values for  $I_P$  gives  $A_\eta = -6.9$  and  $A_{\eta'} = 10.6$ . Integrating the amplitude  $A$  over phase space gives the corresponding partial rate  $\Gamma$  for a single neutrino family

$$\Gamma = \frac{\alpha G_F^2 I_{\pi^0}^2 m_{\pi^0}^7 |\langle \pi^0 | \mathcal{H} | K^0 \rangle|^2}{60(2\pi)^6 (m_K^2 - m_{\pi^0}^2)^2} (1 + A_\eta + A_{\eta'})^2, \quad (8)$$

where  $\alpha = e^2/4\pi$  is the fine structure constant. For three neutrino families, we find using Eq. (8) a branching ratio of  $0.8 \times 10^{-17}$ .

### B. $K_L \rightarrow K^*(\gamma) \rightarrow \nu\bar{\nu}$

The second long-distance contribution we consider is shown in Fig. (1)(b). The diagram involves a radiative transition of the kaon to an intermediate  $K^*$ . The corresponding amplitude  $A$  takes the form

$$A = \frac{(\langle \nu\bar{\nu} | \mathcal{H} | K^{*0} \rangle + \langle \nu\bar{\nu} | \mathcal{H} | \bar{K}^{*0} \rangle) \cdot \langle K^{*0} \gamma | \mathcal{H} | K^0 \rangle}{\sqrt{2}(q^2 - m_{K^*}^2)}, \quad (9)$$

assuming  $\langle \bar{K}^{*0} \gamma | \mathcal{H} | \bar{K}^0 \rangle = \langle K^{*0} \gamma | \mathcal{H} | K^0 \rangle$ . To model the photon vertex, we normalize the amplitude predicted by the vector meson dominance hypothesis to the experimental rate for  $K^* \rightarrow K^0 \gamma$ . The amplitude is [12]

$$A_{K^* \rightarrow K^0 \gamma} = eg \varepsilon_{\mu\nu\rho\sigma} q^\mu E^\nu k^\rho \epsilon^\sigma, \quad (10)$$

where  $g$  is the effective vertex coupling. The corresponding decay rate is

$$\Gamma_{K^* \rightarrow K^0 \gamma} = \frac{\alpha |g|^2 m_{K^*}^3}{24} \left( 1 - \frac{m_{K^0}^2}{m_{K^*}^2} \right)^3. \quad (11)$$

The measured branching ratio for  $K^* \rightarrow K^0 \gamma$  is  $2.3 \times 10^{-3}$  [13]. This implies  $|g| = 1.3$  GeV<sup>-1</sup>.

The  $K^* \rightarrow \nu\bar{\nu}$  transition is modelled as a short-distance process. In the standard model, the quark-level interaction  $d\bar{s} \rightarrow \nu\bar{\nu}$  proceeds at the one-loop level. As indicated in Fig. 3, both box and effective  $dsZ$  vertex diagrams contribute. The corresponding effective four-fermion interaction is [3]

$$\mathcal{H}_i = 2\sqrt{2}G_F\chi\tilde{D}_i\bar{s}\gamma_\mu P_L d\bar{\nu}_i\gamma^\mu P_L\nu_i + \text{h.c.}, \quad (12)$$

where  $\chi = \alpha/4\pi\sin^2\theta_W$  and  $i = e, \mu, \tau$  denotes the neutrino family. The quantity  $\tilde{D}_i$  is a function of the appropriate lepton mass, the up-type quark masses, and several elements of the Kobayashi-Maskawa matrix. Our determinations for  $\tilde{D}_i$  are described in the Appendix. The  $K^*$  transitions determined by  $\mathcal{H}_i$  contain the hadronic matrix element  $\langle 0|\bar{s}\gamma_\mu P_L d|K^*\rangle \equiv f_{K^*}E_\mu$ . We will take  $f_{K^*} = f_\rho = (0.2)m_\rho^2$  [14].

Eqs. (10) and (12) determine all the transition elements appearing in Eq. (9). The resulting amplitudes  $A_i$  for a single neutrino family are

$$A_i = \frac{4egG_F\chi f_{K^*}\text{Re}\tilde{D}_i}{q^2 - m_{K^*}^2}\varepsilon^{\mu\nu\rho\sigma}(\bar{u}_i\gamma_\mu P_L v_i)k_\nu\epsilon_\rho p_\sigma. \quad (13)$$

The corresponding partial decay rates are

$$\Gamma_i = \frac{\alpha|g|^2(G_F\chi f_{K^*}\text{Re}\tilde{D}_i)^2 m_K^3}{12\pi^2}F(x), \quad (14)$$

where  $x = m_{K^*}^2/m_K^2$  and  $F(x)$  is a kinematic function. Specifically,

$$F(x) = -\frac{17}{6} + 7x - 4x^2 - (x-1)^2(4x-1)\ln\frac{x-1}{x}.$$

Summing over the three neutrino families gives  $\Gamma = 8.5 \times 10^{-30}$  GeV, or a branching ratio of  $0.7 \times 10^{-12}$ .

### III. SHORT-DISTANCE

For  $K_L \rightarrow \gamma\nu\bar{\nu}$ , the relevant short-distance interaction is  $d\bar{s} \rightarrow \gamma\nu\bar{\nu}$ . To classify the lowest order diagrams, it is convenient to start with the graphs for  $d\bar{s} \rightarrow \nu\bar{\nu}$ . These were shown earlier in Fig. 3. Adding a photon to any charged line creates a graph for  $d\bar{s} \rightarrow \gamma\nu\bar{\nu}$ . Provided the standard-model  $WWZ\gamma$  vertex is included, this method generates the full set of lowest order diagrams. The short-distance contributions thus naturally split into box (Fig. 4) and effective  $dsZ$  type (Fig. 5) diagrams. Each class further divides into one-particle irreducible and one-quark reducible processes.

Ma and Okada [6] only considered the leading contribution to the effective  $dsZ$  type diagrams: the one-particle irreducible graphs containing a single  $W$  boson [2]. Assuming just two quark families, they found the following short-distance amplitude for  $K_L \rightarrow \gamma\nu\bar{\nu}$ :

$$\frac{\sqrt{2}eG_F^2\sin\theta_c\cos\theta_c c_V u f_K}{3\pi^2}\varepsilon^{\mu\nu\rho\sigma}(\bar{u}\gamma_\mu P_L v)k_\nu\epsilon_\rho p_\sigma, \quad (15)$$

where  $\theta_c$  is the Cabibbo angle. Their result was dominated by the graphs containing an intermediate  $u$  quark. The heavier charm quark contributions were shown to be small. The analysis, however, did not take into account the possibility of an intermediate quark mass larger than the  $W$  mass.

We have extended the Ma and Okada calculation to the case of three fermion families, and a large top quark mass. In the large mass approximation, the above amplitude would be modified by the factor

$$\frac{p \cdot k}{6m_W^2} \frac{V_{td}V_{ts}^*}{\sin \theta_c \cos \theta_c} \left[ \frac{2}{(z-1)^2} - \frac{2 \ln z}{(z-1)^3} - \frac{1}{z(z-1)} \right],$$

where  $z = m_t^2/m_W^2$ . For  $m_t \approx 174$  GeV [15], this factor actually reduces the corresponding rate by several orders of magnitude. Thus Ma and Okada's conclusion that the effective  $dsZ$  diagrams are dominated by the lightest quark is still valid.

Ma and Okada, however, did not consider the box diagram contributions. Our expectation is that the major short-distance contributions in fact come from the one-quark reducible box diagrams in Fig. 4(b).

In order to later treat non-standard model effects, we approach the calculation in a relatively general manner. As indicated in Fig. 6, we consider all one-quark reducible processes that can be viewed as a photon attached to some effective  $d\bar{s} \rightarrow \nu_j \bar{\nu}_k$  interaction. The form of the four-fermion Hamiltonian is taken to be

$$\mathcal{H} = \beta_{jk} \bar{s} D^\mu d \bar{\nu}_j N_\mu \nu_k + \text{h.c.}, \quad (16)$$

where  $D_\mu \equiv \gamma_\mu(\mathbf{v}_D - \mathbf{a}_D \gamma_5)$  and  $N_\mu \equiv \gamma_\mu(\mathbf{v}_N - \mathbf{a}_N \gamma_5)$  are arbitrary mixtures of vector and axial-vector components. The standard-model effective four-fermion Hamiltonian was discussed previously in Eq. (12). In this case, the fermion currents are both left-handed, lepton number conservation implies  $\beta_{j \neq k} = 0$ , and  $\beta_{jj} = 2\sqrt{2}G_F \chi \tilde{D}_j$ . Note that by using these coefficients, several effective  $dsZ$  type graphs will be included along with the one-quark reducible box diagrams.

Using the interaction  $\mathcal{H}$ , the quark-level amplitude generated by the processes in Fig. 6 is

$$A = \frac{e\beta_{jk}}{6} \bar{v}_s \left[ \frac{D^\mu (\not{p}_d - \not{k} + m_d) \not{\epsilon}}{p_d \cdot k} + \frac{\not{\epsilon} (\not{p}_s - \not{k} + m_s) D^\mu}{p_s \cdot k} \right] u_d \bar{u}_j N_\mu v_k, \quad (17)$$

where  $m_d$  and  $m_s$  are quark current masses. It remains to extract the corresponding kaon decay amplitude. For a reasonable estimate we project out the ‘‘pseudoscalar’’ content of  $A$  with the operation [16]

$$M = \mathcal{C} \sum \bar{u}_s \gamma^5 v_d A, \quad (18)$$

where the sum is over the quark spins and  $\mathcal{C}$  is a normalization constant. Only terms that conserve  $CP$  are retained. In addition a simple static constituent quark model is used to evaluate the quark momenta. The resulting projected amplitude for  $K^0 \rightarrow \gamma \nu_j \bar{\nu}_k$  is

$$M = \frac{4\mathcal{C}e\beta_{jk}}{3p \cdot k}(m_s - m_d)\mathbf{v}_D \varepsilon^{\mu\rho\nu\sigma}(\bar{\nu}_j N_\mu \nu_k)k_\rho \epsilon_\nu p_\sigma \quad (19)$$

where  $m_d$  and  $m_s$  are now constituent quark masses. The  $\bar{K}^0$  amplitude is identical except that  $\beta_{jk}^*$  appears. Notice that only the vector part of the quark current contributes.

The normalization constant  $\mathcal{C}$  is determined by applying the projection to the decay  $K^+ \rightarrow l^+ \nu_l$ . Comparison with the definition of the kaon decay constant gives  $\mathcal{C} = f_K m_K / 8m_s m_d V_{us}^*$ .

After combining the  $K^0$  and  $\bar{K}^0$  amplitudes, and integrating over phase space, we obtain the corresponding  $K_L \rightarrow \gamma \nu \bar{\nu}$  decay rate

$$\Gamma = \frac{\alpha}{2(72\pi)^2}(\mathbf{v}_N^2 + \mathbf{a}_N^2)\mathbf{v}_D^2 \text{Tr}[(\beta + \beta^\dagger)^2] \frac{f_K^2 \rho^2 m_K^3}{|V_{us}|^2}, \quad (20)$$

where  $\rho \equiv m_s/m_d - m_d/m_s$ . Inserting the standard-model couplings and coefficient matrix  $\beta$  gives

$$\Gamma = \frac{2\alpha G_F^2 \chi^2}{(72\pi)^2} \sum_i (\text{Re} \tilde{D}_i)^2 \frac{f_K^2 \rho^2 m_K^3}{|V_{us}|^2}. \quad (21)$$

Our numerical evaluation of the Inami and Lim function  $\tilde{D}_i$  is discussed in the Appendix. Estimates for the constituent quark masses vary substantially. We will take  $\rho = 0.8 \pm 0.2$  to account for some of this uncertainty. The remaining parameters are all well-known [13]. The resulting branching ratio is  $0.7_{-0.4}^{+0.6} \times 10^{-11}$ .

#### IV. HORIZONTAL GAUGE BOSONS

Since  $K_L \rightarrow \gamma \nu \bar{\nu}$  is highly suppressed in the standard model, observation of this decay at a higher rate would signal new physics. Therefore, it is of interest to look at the predictions of extended models. One possibility is the contribution of flavor-changing neutral currents (FCNC). Here we consider the effects of neutral generation-changing gauge bosons and, in particular, we follow the general formalism adopted by Cahn and Harari [17]. We have extended this formalism to three generations, as follows.

The general group structure is taken to be  $G \times H$ , where  $G$  acts within a generation and  $H$  is a ‘‘horizontal’’ gauge group containing neutral generation-changing bosons. The group  $G$  contains the standard electroweak algebra  $\text{SU}(2)_W \times \text{U}(1)$ . The group  $H$  is taken to be  $\text{SU}(2)_H$ . We will further assume that the three horizontal gauge bosons are degenerate in mass.

The basis of particle states is constructed as follows. Let  $L_1^0$ ,  $L_2^0$  and  $L_3^0$  denote the ‘‘primitive’’ electron, muon, and tau. For the present, it is convenient to ignore the distinction between left and right components. These primitive states are eigenstates of both  $\text{SU}(2)_W$  and  $\text{SU}(2)_H$  with eigenvalues  $T_3^W = -1/2$  and  $T_3^H = -1, 0, 1$  respectively. Similarly, let the triplets  $N_i^0$ ,  $U_i^0$  and  $D_i^0$  denote the primitive states of the neutrinos, up-type, and down-type quarks.

The set of mass eigenstates is assumed to be related to the primitive states by a unitary transformation. Specifically,

$$F \equiv \begin{bmatrix} N \\ L \\ U \\ D \end{bmatrix} = \begin{bmatrix} \mathcal{U}^N & & & \\ & \mathcal{U}^L & & \\ & & \mathcal{U}^U & \\ & & & \mathcal{U}^D \end{bmatrix} \begin{bmatrix} N^0 \\ L^0 \\ U^0 \\ D^0 \end{bmatrix} \equiv \mathcal{U}F^0.$$

In the primitive basis, the horizontal currents have the simple representation  $\bar{F}^0 \mathbf{T}^H F^0$  where  $\mathbf{T}^H = \mathbb{1}_4 \otimes \boldsymbol{\tau}$  and the  $\tau_i$  are the generators for the 3-dimensional representation of SU(2). For convenience the Lorentz structure of the currents has been temporarily suppressed. The horizontal gauge bosons thus presumably give rise to the following low-energy effective interaction

$$\mathcal{H} = \frac{g_H^2}{2m_H^2} (\bar{F} \mathcal{U} \boldsymbol{\tau} \mathcal{U}^\dagger F)^2, \quad (22)$$

where  $g_H$  is the gauge coupling constant and  $m_H$  is the mass of the gauge bosons.

For the decay  $K_L \rightarrow \gamma \nu \bar{\nu}$ , the relevant interactions in  $\mathcal{H}$  are those that connect the  $D$  and  $N$  triplets. These can be written as

$$\mathcal{H}_{DN} = \frac{g_H^2}{m_H^2} \bar{D} \boldsymbol{\tau} D \cdot \bar{N} \mathcal{U}^N \mathcal{U}^{D\dagger} \boldsymbol{\tau} \mathcal{U}^D \mathcal{U}^{N\dagger} N, \quad (23)$$

by making the replacement  $\boldsymbol{\tau} \rightarrow \mathcal{U}^{D\dagger} \boldsymbol{\tau} \mathcal{U}^D$ . Furthermore, keeping just the terms involving the  $d$  to  $s$  quark transitions gives

$$\mathcal{H}_{ds} = \frac{g_H^2}{\sqrt{2}m_H^2} (\mathcal{U}^N \mathcal{U}^{D\dagger} \boldsymbol{\tau} \mathcal{U}^D \mathcal{U}^{N\dagger})_{jk} \bar{s} d \bar{\nu}_j \nu_k + \text{h.c.} \quad (24)$$

Comparison of this expression with the general Hamiltonian given in Eq. (16) determines the coefficients  $\beta_{jk}$  that appeared in our short-distance analysis. Thus the decay rate given in Eq. (20) can be used directly. Note that the unitary mixing matrices do not contribute to the trace. The resulting  $K_L \rightarrow \gamma \nu \bar{\nu}$  rate is

$$\Gamma = \frac{2\alpha}{(72\pi)^2} (\mathbf{v}_N^2 + \mathbf{a}_N^2) \mathbf{v}_D^2 \frac{g_H^4}{m_H^4} \frac{f_K^2 \rho^2 m_K^3}{|V_{us}|^2}. \quad (25)$$

The neutral generation-changing bosons that we are considering also mediate the lepton-number violating processes  $K_L \rightarrow e\mu$  and  $K^+ \rightarrow \pi^+ e\mu$ . The stringent experimental limits on these processes help to constrain the horizontal gauge boson couplings and mass. The process  $K_L \rightarrow e\mu$ , however, is only sensitive to the axial-vector component of the quark currents. Thus the semi-leptonic decay  $K^+ \rightarrow \pi^+ e\mu$ , which is sensitive to the vector component, is more convenient as a comparison process.

The relevant quark-level process for  $K^+ \rightarrow \pi^+ e^- \mu^+$  is  $d\bar{s} \rightarrow e^- \mu^+$ . Repeating the steps for the  $DL$  interactions that were used for the  $DN$  interactions, one finds that the appropriate term in the Hamiltonian is

$$\mathcal{H}_{sd\bar{e}\mu} = \frac{g_H^2}{m_H^2} (\mathcal{V}_{e\mu} \mathcal{V}_{\mu\tau}^* + \mathcal{V}_{ee} \mathcal{V}_{\mu\mu}^*) \bar{s} d \bar{e} \mu, \quad (26)$$



where  $\mathcal{V} \equiv \mathcal{U}^L \mathcal{U}^{D\dagger}$  governs the mixing between lepton and down-type quark states. Normalizing the corresponding decay rate to the standard-model decay  $K^+ \rightarrow \pi^0 \nu_\mu \mu^+$  we find the ratio

$$R \equiv \frac{\Gamma_{\pi^+ e^- \mu^+}}{\Gamma_{\pi^0 \nu_\mu \mu^+}} = (v_L^2 + a_L^2) v_D^2 \frac{g_H^4}{m_H^4} \frac{|\mathcal{V}_{e\mu} \mathcal{V}_{\mu\tau}^* + \mathcal{V}_{ee} \mathcal{V}_{\mu\mu}^*|^2}{G_F^2 |V_{us}|^2}.$$

The present experimental limit is  $R < 6.6 \times 10^{-9}$  [13].

The  $K_L \rightarrow \gamma \nu \bar{\nu}$  rate appearing in Eq. (25) can be written in terms of  $R$  as

$$\Gamma = \frac{\alpha G_F^2}{(72\pi)^2} \frac{v_N^2 + a_N^2}{v_L^2 + a_L^2} \frac{f_K^2 \rho^2 m_K^3}{|\mathcal{V}_{e\mu} \mathcal{V}_{\mu\tau}^* + \mathcal{V}_{ee} \mathcal{V}_{\mu\mu}^*|^2} R. \quad (27)$$

In order to obtain a reasonable estimate, we ignore the remaining dependence on horizontal coupling coefficients and mixing angles. We then obtain for  $K_L \rightarrow \gamma \nu \bar{\nu}$  a branching ratio limit of  $\lesssim 2 \times 10^{-11}$ .

## V. CONCLUDING REMARKS

Within the standard model, the decay  $K_L \rightarrow \gamma \nu \bar{\nu}$  is indeed very rare, but not nearly to the extent predicted by earlier calculations [6]. We have found long-distance contributions with branching ratios up to  $0.7 \times 10^{-12}$  and short-distance contributions of  $0.7_{-0.4}^{+0.6} \times 10^{-11}$ . We also considered the possible effects of neutral generation-changing gauge bosons. Present experimental limits for lepton violation suggest that these contributions are limited to  $\lesssim 2 \times 10^{-11}$ .

## VI. ACKNOWLEDGMENT

This work was supported in part by the Natural Science and Engineering Council of Canada.

## APPENDIX:

This appendix discusses the numerical evaluation of the Inami-Lim function  $\tilde{D}_i$  [3]. Values for quantities not specified in the text are taken from the 1994 Review of Particle Properties [13].

### Constraints on the KM Matrix

Since  $\tilde{D}_i$  depends heavily upon the elements of the Kobayashi-Maskawa (KM) matrix, we first update their values [18]. In the Wolfenstein convention [19], to order  $\lambda^3$ , the KM matrix  $V$  takes the form

$$V = \begin{pmatrix} 1 - \lambda^2/2 & \lambda & A\lambda^3(\rho - i\eta) \\ -\lambda & 1 - \lambda^2/2 & A\lambda^2 \\ A\lambda^3(1 - \rho - i\eta) & -A\lambda^2 & 1 \end{pmatrix}. \quad (\text{A1})$$

The measured element magnitudes give  $\lambda = 0.221 \pm 0.002$  and  $A = 0.82 \pm 0.10$ . Furthermore, the ratio  $|V_{ub}/V_{cb}|$  describes a circle in the  $(\rho, \eta)$  plane,

$$\rho^2 + \eta^2 = (0.36 \pm 0.09)^2. \quad (\text{A2})$$

Two additional constraints on  $\rho$  and  $\eta$ , as reviewed below, are obtained from measurements of  $K^0-\bar{K}^0$  and  $B_d^0-\bar{B}_d^0$  mixing.

In the neutral  $B_d$  meson system, mixing is characterized by the parameter  $\chi_d$ . The dominant processes are box diagrams containing top quarks. One obtains [20]

$$\chi_d \simeq \frac{G_F^2 m_W^2}{6\pi^2} f_B^2 B_B m_B \tau_B |\bar{E}(x_t)| \eta_B |V_{tb} V_{td}|^2, \quad (\text{A3})$$

where the function  $\bar{E}(x)$  denotes  $\bar{E}(x, x)$ , and [3]

$$\begin{aligned} \bar{E}(x, y) = \frac{xy}{4} \left[ \frac{y^2 - 8y + 4}{(y-1)^2(x-y)} \ln y \right. \\ \left. + \frac{3}{2(x-1)(y-1)} + (x \leftrightarrow y) \right]. \end{aligned} \quad (\text{A4})$$

The arguments  $x_q = m_q^2/m_W^2$  where  $m_q$  are the quark masses. In the Wolfenstein convention, Eq. (A3) describes a second circle in the  $(\rho, \eta)$  plane,

$$(1 - \rho)^2 + \eta^2 = (1.19 \pm 0.29)^2, \quad (\text{A5})$$

where we used  $f_B = 0.140 \pm 0.025$  GeV and  $B_B = 0.85 \pm 0.10$  [21] for the hadronic parameters,  $m_t = 174 \pm 16$  GeV [15] for the top mass, and  $\eta_B = 0.85 \pm 0.05$  [21] for the QCD correction.

In the neutral kaon system, mixing is characterized by the  $CP$  violation parameter  $\epsilon$ . Both charm and top quark box diagrams contribute. One finds [22]

$$|\epsilon| \simeq \frac{G_F^2 m_W^2}{12\pi^2} \frac{f_K^2 B_K m_K}{\sqrt{2} \Delta m_K} \left| \sum_{\substack{i=c,t \\ j=c,t}} \bar{E}(x_i, x_j) \eta_{ij} \text{Im} \Lambda_i \Lambda_j \right|,$$

where  $\Lambda_q$  denotes the product  $V_{qd} V_{qs}^*$ . Note that when evaluating the  $\Lambda_q$ , the KM matrix elements must be expanded to order  $\lambda^5$ . Using  $B_K = 0.7 \pm 0.2$  and  $f_K = 0.160$  GeV [23] for the hadronic factors gives the hyperbola

$$\eta = \frac{(7.3 \pm 2.1) \times 10^{-4}}{A^2 |\eta_{cc} \bar{E}(x_c) - \eta_{ct} \bar{E}(x_c, x_t) - A^2 \lambda^4 (1 - \rho) \eta_{tt} \bar{E}(x_t)|}. \quad (\text{A6})$$

For calculations, the charm mass was taken to be  $m_c = 1.5 \pm 0.1$  GeV, and we used  $\eta_{cc} = 0.76$ ,  $\eta_{ct} = 0.36$ , and  $\eta_{tt} = 0.61$  [23] for the QCD corrections.

The one-sigma contours for the constraints (A2), (A5), and (A6) are plotted in Fig. 7. The product of these distributions determines our expected region for  $\rho$  and  $\eta$ . Contours for this region are shown in Fig. 8.

### Evaluation of $\tilde{D}_i$

In the Wolfenstein convention for the KM matrix, the function  $\tilde{D}_i$ ,  $i \in \{e, \mu, \tau\}$ , becomes

$$\tilde{D}_i \simeq -\lambda\eta_c\bar{D}(x_c, y_i) - \lambda^5\eta_t A^2(1 - \rho - i\eta)\bar{D}(x_t, y_i),$$

where  $\eta_c$  and  $\eta_t$  are QCD corrections and

$$\begin{aligned} \bar{D}(x, y) = \frac{x}{8} \left\{ \left[ \frac{y}{x-y} \left( \frac{y-4}{y-1} \right)^2 \ln y + (x \leftrightarrow y) \right] \right. \\ \left. + 2 - 3 \frac{y+2}{(y-1)(x-1)} + \frac{x^2 - 2x + 4}{(x-1)^2} \ln x \right\} \end{aligned} \quad (\text{A7})$$

For the standard-model masses  $y \ll 1$ , and  $y \ll x$  except when  $y = y_\tau$  and  $x = x_c$ . It follows that  $\tilde{D}_i$  is relatively insensitive to  $i$ . We again take  $m_c = 1.5 \pm 0.1$  GeV and  $m_t = 174 \pm 16$  GeV, and set  $\eta_c = 0.7$  and  $\eta_t = 1$  [24]. Then using the Wolfenstein parameter values determined above, we find

$$\begin{aligned} \text{Re}\tilde{D}_{e,\mu} &= -1.8_{-0.3}^{+0.5} \times 10^{-3}, \\ \text{Re}\tilde{D}_\tau &= -1.6_{-0.3}^{+0.6} \times 10^{-3}, \\ \text{Im}\tilde{D}_i &= 3.0_{-1.3}^{+2.0} \times 10^{-4}. \end{aligned} \quad (\text{A8})$$

The listed values are the modes and the uncertainties enclose 68.3% of the distributions.

## REFERENCES

- [1] For reviews, see J. L. Ritchie and S. G. Wojcicki, *Rev. Mod. Phys.* **65**, 1149 (1993); L. Littenberg and G. Valencia, *Annu. Rev. Nucl. Part. Sci.* **43**, 729 (1993); R. Battiston, D. Cocolicchio, G. L. Fogli, and N. Paver, *Phys. Rep.* **214**, 293 (1992); J. S. Hagelin and L. S. Littenberg, *Prog. Nucl. Part. Phys.* **23**, 1 (1989).
- [2] M. K. Gaillard and B. W. Lee, *Phys. Rev. D* **10**, 897 (1974).
- [3] T. Inami and C. S. Lim, *Prog. Theor. Phys.* **65**, 297 (1981); **65** 1772(E) (1982).
- [4] M. S. Atiya *et. al.*, *Phys. Rev. D* **48**, 1 (1993); D. Rein and L. M. Sehgal, *Phys. Rev. D* **39**, 3325 (1989); J. Ellis, J. S. Hagelin, and S. Rudaz, *Phys. Lett. B* **192**, 201 (1987).
- [5] L. S. Littenberg, *Phys. Rev. D* **39**, 3322 (1989); J. Ellis, M. K. Gaillard, and D. V. Nanopoulos, *Nucl. Phys.* **B109**, 213 (1976).
- [6] E. Ma and J. Okada, *Phys. Rev. D* **18**, 4219 (1978).
- [7] J. F. Donoghue, B. R. Holstein, and Y.-C. R. Lin, *Nucl. Phys.* **B277**, 651 (1986).
- [8] C. Picciotto, *Phys. Rev. D* **45**, 1569 (1992).
- [9] D. Grasso and M. Lusignoli, *Phys. Lett. B* **279**, 161 (1992); L. Arnellos, W. J. Marciano, and Z. Parsa, *Nucl. Phys.* **B196**, 365 (1982).
- [10] For example, see B. de Wit and J. Smith, *Field Theory in Particle Physics* (North-Holland Physics Publishing, New York, 1986).
- [11] J. F. Donoghue, B. R. Holstein, and Y.-C. R. Lin, *Phys. Rev. Lett.* **55**, 2766 (1985).
- [12] For example, see J. W. Durso, *Phys. Lett. B* **184**, 348 (1987).
- [13] Particle Data Group, *Phys. Rev. D* **50**, 1173 (1994).
- [14] For example, see J. F. Donoghue, E. Golowich, and B. R. Holstein, *Dynamics of the Standard Model* (Cambridge University Press, Cambridge, 1992).
- [15] CDF Collaboration, *Phys. Rev. Lett.* **73**, 225 (1994).
- [16] T. Goldman and W. J. Wilson, *Phys. Rev. D* **15**, 709 (1977).
- [17] R. N. Cahn and H. Harari, *Nucl. Phys.* **B176**, 135 (1980).
- [18] For similar treatments, see J. M. Soares and L. Wolfenstein, *Phys. Rev. D* **47**, 1021 (1993); G. Bélanger and C. Q. Geng, *Phys. Rev. D* **43**, 140 (1991).
- [19] L. Wolfenstein, *Phys. Rev. Lett.* **51**, 1945 (1983).
- [20] G. Altarelli and P. J. Franzini, *Z. Phys. C* **37**, 271 (1988).
- [21] C. S. Kim, J. L. Rosner, and C. P. Yuan, *Phys. Rev. D* **42**, 96 (1990).
- [22] E. A. Paschos and U. Türke, *Phys. Rep.* **178**, 145 (1989).
- [23] G. Bélanger and C. Q. Geng, *Phys. Rev. D* **43**, 140 (1991).
- [24] G. Buchalla and A. J. Buras, *Nucl. Phys.* **B412**, 106 (1994).

## FIGURES

FIG. 1. Long-distance contributions.

FIG. 2. Triangle diagram for the pseudoscalar decays  $P \rightarrow \gamma\nu\bar{\nu}$ . The effect of the diagram with the photon and  $Z$  lines interchanged is to double the weak vector couplings  $c_{Vq}$  and cancel the weak axial-vector couplings  $c_{Aq}$ .

FIG. 3. Diagrams for  $d\bar{s} \rightarrow \nu\bar{\nu}$ . The four effective  $dsZ$  vertex diagrams can be classified as either (a) one-particle irreducible or (b) one-quark reducible. Only one of each pair is drawn. (c) The box diagram.

FIG. 4. The box diagrams for  $d\bar{s} \rightarrow \gamma\nu\bar{\nu}$  can be generated from the box diagram for  $d\bar{s} \rightarrow \nu\bar{\nu}$  by photon emission from all charged lines. Shown here are examples of (a) one-particle irreducible and (b) one-quark reducible graphs.

FIG. 5. Effective  $dsZ$  diagrams for  $d\bar{s} \rightarrow \gamma\nu\bar{\nu}$  can be generated from the effective  $dsZ$  diagrams for  $d\bar{s} \rightarrow \nu\bar{\nu}$  by photon emission from all charged lines. Shown here are examples of (a) one-particle irreducible and (b) one-quark reducible graphs.

FIG. 6. Effective short-distance processes.

FIG. 7. One-sigma constraint curves for  $\rho$  and  $\eta$ . The dashed and dotted lines respectively are the  $V_{ub}/V_{cb}$  and  $B$  mixing circles. The solid lines are generated from the  $K$  mixing hyperbola by a Monte Carlo treatment of the uncertainties.

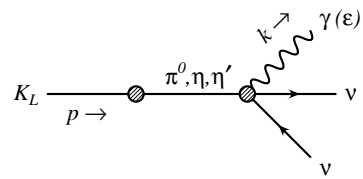
FIG. 8. Expected  $(\rho, \eta)$  region. Dashed contour encloses 68.3% of the distribution; solid contour encloses 90%.

TABLES

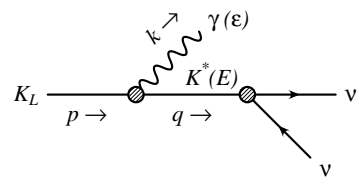
TABLE I. Effective meson-quark couplings.

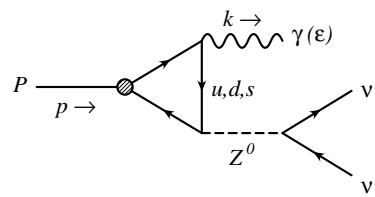
$P$	$g_{P u \bar{u}}/m_u$	$g_{P d \bar{d}}/m_d$	$g_{P s \bar{s}}/m_s$
$\pi^0$	$(2)^{1/2} f_\pi^{-1}$	$-(2)^{1/2} f_\pi^{-1}$	0
$\eta_8$	$(2/3)^{1/2} f_8^{-1}$	$(2/3)^{1/2} f_8^{-1}$	$-(8/3)^{1/2} f_8^{-1}$
$\eta_0$	$2(3)^{-1/2} f_0^{-1}$	$2(3)^{-1/2} f_0^{-1}$	$2(3)^{-1/2} f_0^{-1}$

(a)

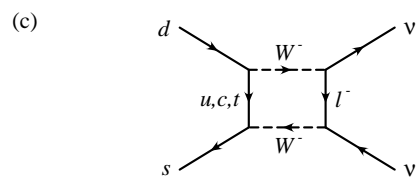
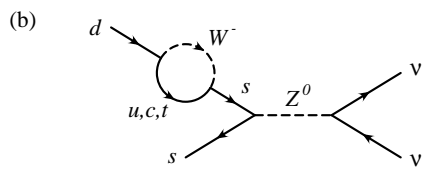
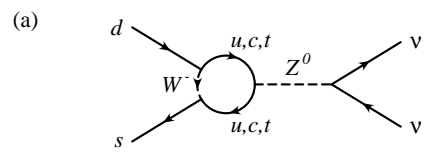


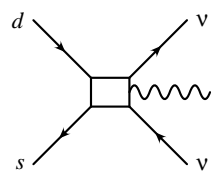
(b)



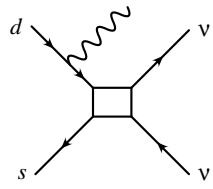








(a)



(b)

